Route to high-T_c superconductivity via CH$_4$-intercalated H$_3$S hydride perovskites

Wenwen Cui [ORCID],[1] Tiange Bi [ORCID],[2] Jingming Shi,[1] Yinwei Li [ORCID],[1,*] Hanyu Liu,[3,4,†] Eva Zurek [ORCID],[2,‡] and Russell J. Hemley [ORCID][5,§]

[1]*Laboratory of Quantum Materials Design and Application, School of Physics and Electronic Engineering,*
Jiangsu Normal University, Xuzhou 221116, China
[2]*Department of Chemistry, State University of New York at Buffalo, Buffalo, New York 14260, USA*
[3]*International Center for Computational Method and Software, College of Physics, Jilin University, Changchun 130012, China*
[4]*International Center of Future Science, Jilin University, Changchun 130012, China*
[5]*Departments of Physics and Chemistry, University of Illinois at Chicago, Chicago, Illinois 60607, USA*

While exploring potential superconductors in the C-S-H ternary system using first-principles crystal structure prediction methods, we uncovered a class of hydride perovskites based on the intercalation of methane into an H$_3$S framework. These intriguing H$_3$S-CH$_4$ structures emerge as metastable at ∼100 GPa. Electron-phonon coupling calculations indicate that phases with CSH$_7$ stoichiometry are potential superconductors with T_c values ranging from 100 K to 190 K at megabar pressures. The results are expected to guide the experimental search for new high-T_c superconductors, including those stable at lower pressures than previously documented superconducting hydrides such as H$_3$S and LaH$_{10}$.

I. INTRODUCTION

The pursuit of high-T_c and even room-temperature superconductivity has been a grand challenge in physics since the 1911 discovery of superconductivity [1]. The Bardeen-Cooper-Schrieffer (BCS) theory [2] can describe well the mechanism for conventional superconductors, opening the door for the discovery and design of high-T_c materials. Ashcroft [3] proposed that compressed hydrides are good candidates for high-T_c superconductors due to chemical "precompression" effects. Subsequent theoretical studies provided explicit predictions of these phenomena, and they have led to the discovery of very high temperature superconductivity, first in H$_3$S (T_c of 203 K) [4] and more recently in LaH$_{10}$ (T_c up to 260 K) [5–7]. These experimental results confirmed theoretical predictions for both the structures and basic mechanism of superconductivity [8–11], thereby marking a new era for both superconductivity and "materials by design" [5,12–14].

Compared to binary hydrides, exploration of high-T_c superconductors in ternary hydrides greatly enlarges the configurational space and opens up new chemistry and physics that could in principle enhance both T_c and stability, including at modest pressures. This additional elemental degree of freedom in compressed ternary hydride systems has led to new predicted high-T_c superconductors such as CaYH$_{12}$ ($T_c = 258$ K at 200 GPa) [15], LiPH$_6$ ($T_c = 150$–167 K at 200 GPa) [16], and most remarkably Li$_2$MgH$_{16}$ ($T_c = 473$ K at 250 GPa) [17]. On the other hand, existing experimental studies have uncovered only relatively low-T_c materials

such as in BaReH$_9$ ($T_c = 7$ K) [18] and Li$_5$MoH$_{11}$ ($T_c = 6.5$ K) [19]. Returning to sulfur-containing systems, carbon disulfide (CS$_2$) has been shown to transform to a metal at 50 GPa, and a superconductor with a T_c of ∼6 K at 60–170 GPa [20]. Several ternary hydrides based on the H$_3$S structure are predicted to exhibit high-T_c behavior, including H$_6$SSe (i.e., SH$_3$-SeH$_3$, with an estimated T_c of 195 K at 200 GPa) [21], Y(La)SH$_6$ [SH$_3$-Y(La)H$_3$, $T_c = 95$ and 35 K at 210 and 300 GPa, respectively] [22], and even the noble gas Xe with H$_3$S (H$_3$SXe, $T_c = 89$ K at 240 GPa) [23]. Moreover, several superconductors have also been reported in ternary F-S-H, Y-S-H, and B-S-H compounds [24–26].

There is also general interest in carbon-containing high-T_c superconductors. Dense carbides that are isostructural with hydrides have been predicted to exhibit high-T_c behavior and to be stable on decompression due to their rigid carbon sp^3 frameworks [27]. Various hydrocarbons (e.g., CH$_4$, C$_2$H$_4$, and C$_2$H$_6$) are stable in different molecular phases to megabar pressures [28–30]. CH$_4$ and Mg are predicted to form CH$_4$Mg, a potential superconductor with a T_c of 84–121 K at 75–120 GPa [31]. The related compound CH$_4$K has a predicted T_c of about 12 K at 80 GPa [32]. These results encouraged us to theoretically search for high-T_c superconductors in the C-S-H ternary system. As shown in detail below, *Cm*, *R*3*m*, and *Pnma* symmetry phases were found, for which electron-phonon coupling calculations reveal superconductivity with T_c's as high as 194 K at 150 GPa, as estimated by solving the Eliashberg equations numerically using the typical choice of the Coulomb potential, $\mu^* = 0.10$–0.13.

II. RESULTS AND DISCUSSION

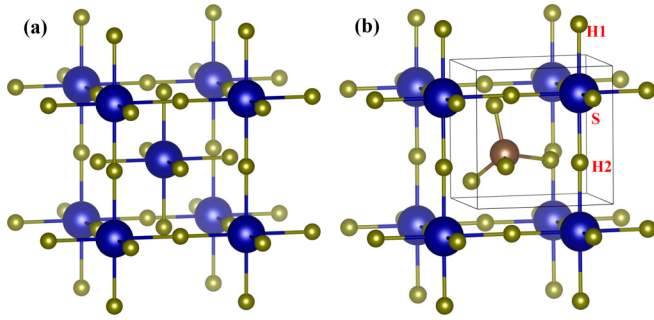We began by identifying stable structures in the C-S-H system, focusing on C$_x$S$_y$H$_z$ ($x = 1 - 2$; $y = 1 - 2$; $z = 1 - 8$) compositions at megabar pressures (100–200 GPa),

FIG. 1. (a) H_3S ($Im\bar{3}m$ structure) and (b) $R3m$ symmetry methane intercalated H_3S perovskite, CSH_7. The brown, blue, and yellow-green spheres denote C, S, and H atoms, respectively (see the supplemental material [37] for more detailed structural information).

using heuristic algorithms based on particle swarm optimization [33–35] and evolutionary algorithms [36] in combination with first-principles theory [computational details are provided in the supporting information (SI) [37]]. The CSH_7 stoichiometry emerged as being particularly stable relative to the elements in the pressure range considered. The enthalpies of formation from the elemental phases for CSH_7 were −70, −62, −53, and −30 meV/at at 100, 130, 150, and 200 GPa, respectively. Interestingly, the structures of CSH_7, shown in Fig. S1 of the SI, are composed of CH_4 molecules intercalated within different, but related, H_3S networks. At 100 GPa, the H_3S sublattice is characterized by SH_5 layers. Upon compression perovskite structures derived from the phase shown in Fig. 1 become enthalpically favored, with CH_4 molecules intercalated into the cubic H_3S framework formed by two neighboring SH_5 layers that are linked via shared H atoms.

Although the enthalpies of formation of the CSH_7 phases are negative with respect to the elemental phases, these species do not lie on the 3D convex hull. In fact, they are metastable with respect to $CH_4 + H_3S$ (and $CH_4 + H_2S + 1/2H_2$), but stable relative to $H_2S + C + 5/2H_2$ below 188 GPa. The zero-point energy (ZPE) uncorrected enthalpy of $R3m$ is 33 meV/at above the convex hull at 130 GPa. As shown in Table S1 of the SI, inclusion of the ZPE or finite-temperature effects does not stabilize the ternary phase. It should, however, be noted that a number of compressed hydrides found to be metastable via first-principles calculations have been synthesized in the laboratory. Examples include a Ca_2H_5 phase, which was calculated to be 20 meV/at above the convex hull [38], and hydrides of phosphorus, which are at least 30 meV/at above the convex hull [39–41]. Moreover, these phases could potentially be stabilized by anharmonic or nuclear quantum effects as found for LaH_{10} [42]. Therefore, it is expected that the CSH_7 phases could be realized experimentally, especially if they are calculated to be dynamically stable.

The relative enthalpies of the CSH_7 phases between 100 and 300 GPa are shown in Fig. S2. The small differences in the static lattice enthalpies calculated for these hydride perovskites suggests there may be many other phases, differing in the number of atoms in the formula unit and rotations of the methane molecules, that could be realized. Phonon calculations reveal that Cm is dynamically stable from 100

to 110 GPa, whereas $R3m$ is dynamically stable from 130 to 300 GPa, and $Pnma$ is dynamically stable at the current level of approximation from at least 150 to 300 GPa (Fig. S3). Molecular-dynamics simulations (Fig. S4), suggest that at finite temperature the methane molecules may become rotationally disordered.

Predicted 0 K structures of CSH_7 and cubic $Im\bar{3}m$ H_3S are shown in Fig. 1 and Fig. S1. In pure H_3S, the S atoms form a bcc lattice with each S atom octahedrally coordinated by H atoms [Fig. 1(a)]. The CSH_7 phases are based on the H_3S structure with the central SH_6 unit replaced by a CH_4 molecule, and a distortion of the cubic framework. In the Cm phase [Fig. S1(a)], the cubic H_3S lattice is replaced by two layers of SH_5. The H-S distance between neighboring SH_5 layers is too long (1.906 Å) to form an H-S covalent bond. In the $R3m$ structure, for example, the H_3S framework is retained but with a slight rhombohedral distortion such that the $\vec{a}$, $\vec{b}$, and $\vec{c}$ unit-cell vectors are equal in length, but the α, β, and γ angles measure 89.4° (instead of 90°). The rotation barrier of the CH_4 unit in $R3m$-CSH_7 was estimated to be <1 meV/at at 150 GPa (Fig. S5), suggesting the molecule may exhibit rotational disorder, and that this may occur in other structures, consistent with the molecular dynamics simulations (Fig. S4).

To explore the bonding in the CSH_7 phases, their electronic localization functions (ELFs) were plotted (Fig. S6). The ELF is useful for visualizing covalent bonds and lone pairs; it maps values in the range from 0 to 1, where 1 corresponds to perfect localization of the valence electrons indicative of a strong covalent bond. The ELF values for the S-H and C-H bonds are close to 0.9, indicating their strong covalent character. The Cm structure is characterized by five S-H bonds (bond lengths of 1.38–1.55 Å) and one lone electron pair [Figs. S6(a) and S6(b)]. Similar to free methane, the CH_4 units contain four strong covalent C-H bonds, as shown in the three-dimensional ELF plots. In the $R3m$ and $Pnma$ structure, the cubic H_3S framework (i.e., $Pm\bar{3}m$) is clearly evident.

The calculated pressure-volume equation of states (EOS) of CSH_7 and assemblages consisting of CH_4 and H_3S, as well as $C + S + 7/2H_2$, are shown in Fig. 2. The sum of the volume of the predicted CH_4 ($Cmca$) [43] and H_3S ($R3m$ and $Im\bar{3}m$) [9] phases is also plotted for comparison. The evolution of the volume under pressure of CSH_7 falls between the experimental and theoretical data obtained for $CH_4 + H_3S$. As shown in Fig. S7, the PV contribution to the enthalpy favors the assemblages over CSH_7 within this pressure range. The pressure dependence of select S-H distances is plotted in Fig. S8. Under pressure the S1-H and S2-H bonds in the Cm phase approach each other, and the S3-H distance decreases, as the phase undergoes pressure-induced bond equalization. Because the CH_4 molecule breaks the symmetry, the S-H1 and S-H2 bonds in the $R3m$ phase differ slightly. Both S-H bonds in $R3m$-CSH_7 are slightly shorter than those calculated for $Im\bar{3}m$ H_3S, whose highest T_c, 203 K, was measured at 155 GPa [4]. If the S-H distance, which can be modulated by the identity of the intercalant molecule as well as the pressure, is an important factor in determining the T_c, it is expected that the maximum value for CSH_7 would be at lower pressures, consistent with the explicit calculations of T_c discussed below.

The band structures and partial densities of states (DOSs) for CSH_7 perovskite structures were calculated to further
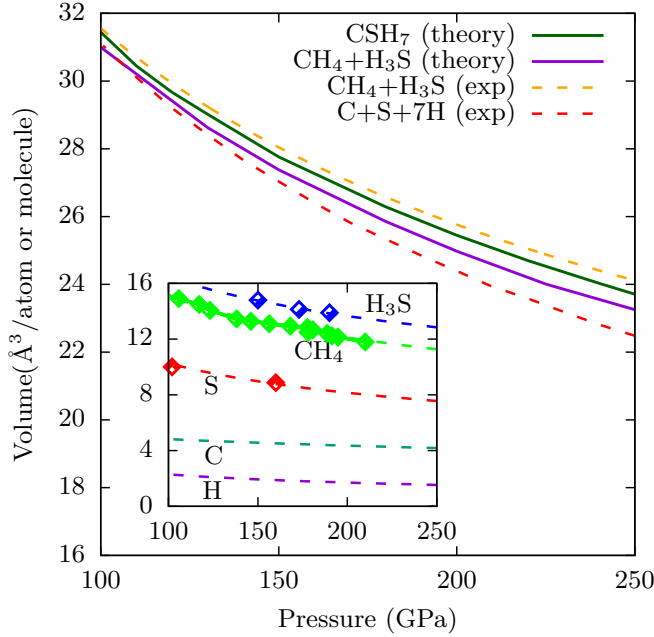
FIG. 2. Calculated CSH$_7$ EOS ($R\bar{m}3$ structure; the volumes of $R3m$ and $Pnma$ are within 0.5%) compared with the molecular assemblage CH$_4$ + H$_3$S, and the assemblage C + S + 7/2H$_2$. The green and violet lines represent theoretical values for CSH$_7$, and the sum of the volume of CH$_4$ ($Cmca$) [43] + H$_3$S ($R3m$ and $Im\bar{3}m$) [9]. The inset shows the experimental EOS for H$_2$ [44], C [45], S [46], CH$_4$ [47], and H$_3$S [48]; the points are the measured data.

explore their electronic properties [Fig. 3(a), Fig. S9(a) and Fig. S10(a)]. They exhibit metallic features, wherein the states near the Fermi level are mainly from the contribution of the H$_3$S framework, with negligible character from the CH$_4$ molecules. The significant overlap of states with H and S character indicates strong H-S hybridization under pressure, which has been demonstrated to play a key role in driving the high-T_c superconductivity of cubic H$_3$S [12].

Figure 3(b), Fig. S9(b) and Fig. S10(b) show the phonon dispersions, projected phonon density of states (PHDOS), Eliashberg spectral function, $\alpha^2F(\omega)$, and electron-phonon coupling integral, $\lambda(\omega)$, for perovskite CSH$_7$. A notable feature of the CH$_4$ intercalation in the structures is the separation of the vibrational modes into three well distinct regions: The lower frequencies (below 20 THz) are associated with the heavier S and C atoms, and modes including some of the CH$_4$ hydrogens; the intermediate frequencies (between 30 and 63 THz) are derived from combinations of H-wagging, bending, and stretching modes; and the higher frequencies ($\sim$100 THz, 3300 cm^{-1}) are derived primarily from the C-H stretching modes of the molecular CH$_4$ units, close to the asymmetric stretching modes of free CH$_4$ ($\sim$97 THz, 3200 cm^{-1}).

The superconducting properties of the CSH$_7$ phases were estimated by the Allen-Dynes modified McMillan equation [49], using typical values of the Coulomb pseudopotential, $\mu^* = 0.13$–0.1. As shown in Table I, below 250 GPa, λ was calculated to be appreciable for all three phases. At 100 GPa, λ was 1.2 and $\omega_{\log}$ was 1091 K for the Cm phase, yielding a T_c of 86–98 K. For $R3m$ at 150 GPa, λ was 2.47,
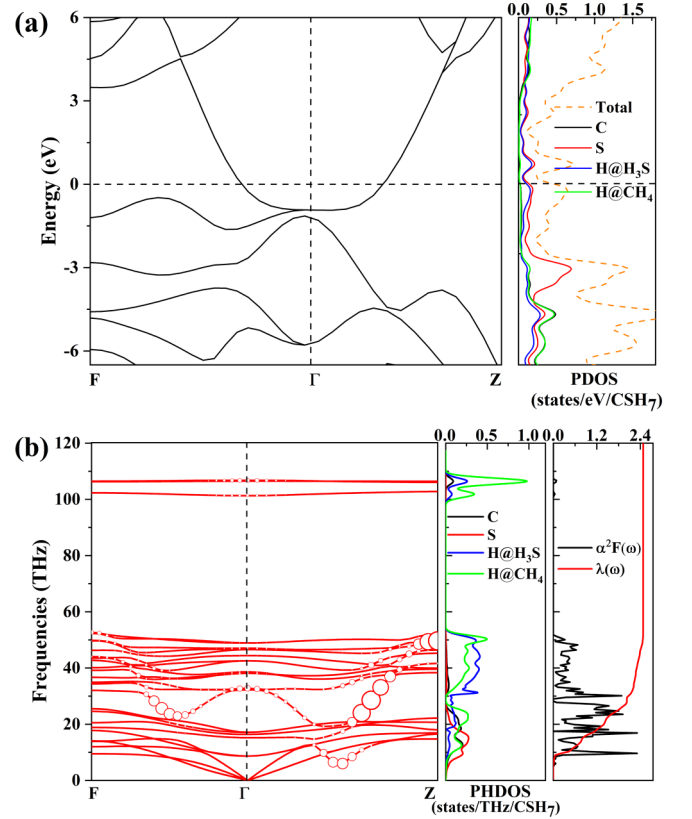

FIG. 3. Calculated (a) band structure, total DOS, and site-projected DOS near the Fermi level, and (b) phonon-dispersion curves, PHDOS, projected on the C, S, and H atoms, Eliashberg spectral function, $\alpha^2F(\omega)$, and $\lambda(\omega) = \int_0^\omega d\omega' 2\alpha^2F(\omega')/(\omega)'$ for CSH$_7$ ($R3m$ structure) at 150 GPa. Red solid circles represent the phonon linewidth with the radius proportional to the respective coupling strength.

which is twice the value found for Cm and comparable to that calculated for cubic H$_3$S at 200 GPa ($\lambda = 2.19$) [9], resulting in a T_c of 143–152 K. The logarithmic average phonon frequency of $R3m$ CSH$_7$ at 150 GPa is somewhat lower than that of $Im\bar{3}m$ H$_3$S at 200 GPa [9], 925 K versus 1335 K, which is the reason for the slightly lower T_c of the ternary. The increase in λ for $R3m$ as compared to Cm is not unreasonable in view of the differences in their phonon band structures. In $R3m$,

TABLE I. The calculated electron-phonon coupling parameter (λ), logarithmic average phonon frequency ($\omega_{\log}$), and the estimated T_c for selected CSH$_7$ structures using the Allen-Dynes modified McMillan (ADM) equation [49], and numerically solving the Eliashberg equations [50] with $\mu^* = 0.10$ (0.13).

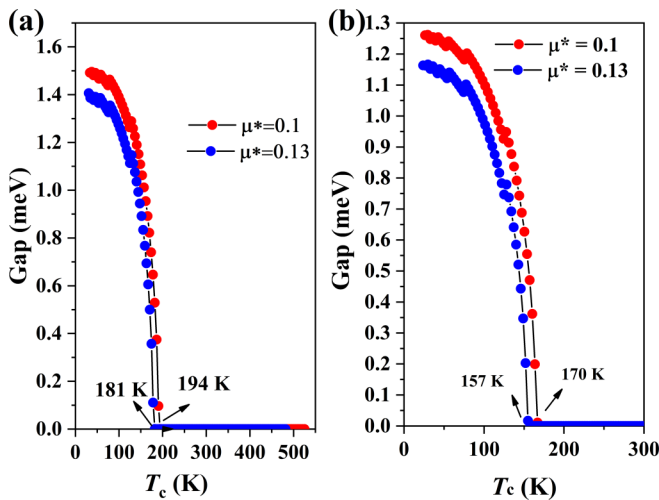|				T_c (K)	
Phase	Pressure (GPa)	λ	$\omega_{\log}$ (K)	ADM	Eliashberg
Cm	100	1.20	1091	98 (86)	108 (97)
$R3m$	150	2.47	925	152 (143)	194 (181)
	200	1.35	1379	137 (128)	158 (144)
$Pmna$	150	3.06	672	122 (116)	170 (157)
	200	1.06	1622	123 (107)	138 (120)

FIG. 4. Calculated anisotropic superconducting gap of CSH_7 in the (a) $R3m$ and (b) $Pnma$ structures at 150 GPa.

there are two obvious Kohn anomalies and softened modes at 18–32 THz located along the F-Γ and Γ-Z high-symmetry lines, which contribute a significant amount ($\sim36\%$) to λ. In addition, λ of $R3m$ and $Pnma$ was found to decrease with increasing pressure, which was not offset by the increase in $\omega_{\log}$ so that T_c decreased from 150 to 300 GPa. The maximum T_c for CSH_7, therefore, occurs at a slightly lower pressure than for H_3S. Notably, it is larger than the highest value computed for H_3SXe, 89 K at 240 GPa [23], because of the smaller mass of CH_4 relative to Xe. For strongly coupled superconductors ($\lambda > 1.5$), Eliashberg theory [50] gives a better estimate of T_c, and therefore we also numerically solved the Eliashberg equations for select pressures, as shown in Table I, Table SII and Fig. 4. As expected, the estimated T_c values were higher, 181–194 and 157–170 K for $R3m$ and $Pnma$, respectively.

III. CONCLUSIONS

In summary, we have explored the stability and electronic properties of $C_xS_yH_z$ ternary compounds at high pressure.

Stoichiometric CSH_7 was found to be dynamically stable above 100 GPa, adopting phases with space-group symmetries based on distortions of the high-symmetry $Pm\bar{3}m$ structure. These perovskite-type structures are characterized by CH_4 intercalated to form distorted H_3S perovskite frameworks, which could represent a new class of high-temperature superconductors. Electron-phonon coupling calculations indicate that CSH_7 phases are promising conventional superconductors with T_c's estimated to be as high as ~200 K. The results are expected to stimulate the search for other high-T_c H_3S intercalation compounds and more chemically complex hydride superconductors, especially in carbon-bearing systems. Just like pressure, the size of the intercalant molecule can be used to modulate the H-S framework, and thereby to tune its properties, such as T_c. Additional theoretical studies would be useful to examine the effects of quantum and anharmonic dynamics on the calculated critical temperatures and stability of this class of materials, as well as mechanisms for enhancing their phase stabilities at lower pressures.

[1] D. Van Delft and P. Kes, Phys. Today **63**(9), 38 (2010).

[2] J. Bardeen, L. N. Cooper, and J. R. Schrieffer, Phys. Rev. **108**, 1175 (1957).

[3] N. W. Ashcroft, Phys. Rev. Lett. **92**, 187002 (2004).

[4] A. Drozdov, M. Eremets, I. Troyan, V. Ksenofontov, and S. Shylin, Nature (London) **525**, 73 (2015).

[5] R. J. Hemley, M. Ahart, H. Liu, and M. Somayazulu, *Proceedings of the International Symposium - Superconductivity and Pressure: A Fruitful Relationship on the Road to Room Temperature Superconductivity - May 21-22, 2018, Madrid, Spain*, edited by M. A. Alario y Franco (Fundación Ramón Areces, Madrid, 2019), pp. 199–213.

[6] M. Somayazulu, M. Ahart, A. K. Mishra, Z. M. Geballe, M. Baldini, Y. Meng, V. V. Struzhkin, and R. J. Hemley, Phys. Rev. Lett. **122**, 027001 (2019).

[7] A. Drozdov, P. Kong, V. Minkov, S. Besedin, M. Kuzovnikov, S. Mozaffari, L. Balicas, F. Balakirev, D. Graf, V. Prakapenka *et al.*, Nature (London) **569**, 528 (2019).

[8] Y. Li, J. Hao, H. Liu, Y. Li, and Y. Ma, J. Chem. Phys. **140**, 174712 (2014).

[9] D. Duan, Y. Liu, F. Tian, D. Li, X. Huang, Z. Zhao, H. Yu, B. Liu, W. Tian, and T. Cui, Sci. Rep. **4**, 6968 (2014).

[10] H. Liu, I. I. Naumov, R. Hoffmann, N. Ashcroft, and R. J. Hemley, Proc. Natl. Acad. Sci. USA **114**, 6990 (2017).

[11] F. Peng, Y. Sun, C. J. Pickard, R. J. Needs, Q. Wu, and Y. Ma, Phys. Rev. Lett. **119**, 107001 (2017).

[12] E. Zurek and T. Bi, J. Chem. Phys. **150**, 050901 (2019).

[13] J. A. Flores-Livas, M. Amsler, C. Heil, A. Sanna, L. Boeri, G. Profeta, C. Wolverton, S. Goedecker, and E. K. U. Gross, Phys. Rev. B **93**, 020508(R) (2016).

[14] P. Cudazzo, G. Profeta, A. Sanna, A. Floris, A. Continenza, S. Massidda, and E. K. U. Gross, Phys. Rev. B **81**, 134506 (2010).

[15] X. Liang, A. Bergara, L. Wang, B. Wen, Z. Zhao, X.-F. Zhou, J. He, G. Gao, and Y. Tian, Phys. Rev. B **99**, 100505(R) (2019).

[16] Z. Shao, D. Duan, Y. Ma, H. Yu, H. Song, H. Xie, D. Li, F. Tian, B. Liu, and T. Cui, npj Comput. Mater. **5**, 1 (2019).

[17] Y. Sun, J. Lv, Y. Xie, H. Liu, and Y. Ma, Phys. Rev. Lett. **123**, 097001 (2019).

[18] T. Muramatsu, W. K. Wanene, M. Somayazulu, E. Vinitsky, D. Chandra, T. A. Strobel, V. V. Struzhkin, and R. J. Hemley, J. Phys. Chem. C **119**, 18007 (2015).

[19] D. Meng, M. Sakata, K. Shimizu, Y. Iijima, H. Saitoh, T. Sato, S. Takagi, and S.-i. Orimo, Phys. Rev. B **99**, 024508 (2019).

[20] R. P. Dias, C.-S. Yoo, V. V. Struzhkin, M. Kim, T. Muramatsu, T. Matsuoka, Y. Ohishi, and S. Sinogeikin, Proc. Natl. Acad. Sci. USA **110**, 11720 (2013).

[21] B. Liu, W. Cui, J. Shi, L. Zhu, J. Chen, S. Lin, R. Su, J. Ma, K. Yang, M. Xu, J. Hao, A. P. Durajski, J. Qi, Y. Li, and Y. Li, Phys. Rev. B **98**, 174101 (2018).

[22] X. Liang, S. Zhao, C. Shao, A. Bergara, H. Liu, L. Wang, R. Sun, Y. Zhang, Y. Gao, Z. Zhao *et al.*, Phys. Rev. B **100**, 184502 (2019).

[23] D. Li, Y. Liu, F.-B. Tian, S.-L. Wei, Z. Liu, D.-F. Duan, B.-B. Liu, and T. Cui, Front. Phys. **13**, 137107 (2018).

[24] S. Zhang, L. Zhu, H. Liu, and G. Yang, Inorg. Chem. **55**, 11434 (2016).

[25] X. Du, S. Zhang, J. Lin, X. Zhang, A. Bergara, and G. Yang, Phys. Rev. B **100**, 134110 (2019).

[26] J. Chen, W. Cui, J. Shi, M. Xu, J. Hao, A. P. Durajski, and Y. Li, ACS Omega **4**, 14317 (2019).

[27] S. Lu, H. Liu, I. I. Naumov, S. Meng, Y. Li, J. S. Tse, B. Yang, and R. J. Hemley, Phys. Rev. B **93**, 104509 (2016).

[28] R. J. Hemley and H.-K. Mao, New findings in static high-pressure science, in *AIP Conference Proceedings No. 706*, edited by M. D. Furnish, Y. M. Gupta, and J. W. Forbes (AIP, New York, 2004), pp. 17–28.

[29] X.-D. Wen, L. Hand, V. Labet, T. Yang, R. Hoffmann, N. Ashcroft, A. R. Oganov, and A. O. Lyakhov, Proc. Natl. Acad. Sci. USA **108**, 6833 (2011).

[30] H. Liu, I. I. Naumov, and R. J. Hemley, J. Phys. Chem. Lett. **7**, 4218 (2016).

[31] F. Tian, D. Li, D. Duan, X. Sha, Y. Liu, T. Yang, B. Liu, and T. Cui, Mater. Res. Express **2**, 046001 (2015).

[32] J.-X. Han, H. Zhang, G.-H. Zhong *et al.*, Int. J. Mod. Phys. C **30**, 1 (2019).

[33] Y. Wang, J. Lv, L. Zhu, and Y. Ma, Phys. Rev. B **82**, 094116 (2010).

[34] Y. Wang, J. Lv, L. Zhu, and Y. Ma, Comput. Phys. Commun. **183**, 2063 (2012).

[35] B. Gao, P. Gao, S. Lu, J. Lv, Y. Wang, and Y. Ma, Sci. Bull. **64**, 301 (2019).

[36] D. C. Lonie and E. Zurek, Comput. Phys. Commun. **182**, 372 (2011).

[37] See Supplemental Material at http://link.aps.org/supplemental/ 10.1103/PhysRevB.101.134504, for details of the computational methods, structures considered in the optimizations, explicit structural information and illustrations of the CSH_7 compounds, as well as additional results on the phase stabilities, the effect of the zero-point energy, and plots related to the electronic structure and computed superconducting properties, which includes Refs. [52–62].

[38] A. K. Mishra, T. Muramatsu, H. Liu, Z. M. Geballe, M. Somayazulu, M. Ahart, M. Baldini, Y. Meng, E. Zurek, and R. J. Hemley, J. Phys. Chem. C **122**, 19370 (2018).

[39] A. Drozdov, M. Eremets, and I. Troyan, arXiv:1508.06224.

[40] A. Shamp, T. Terpstra, T. Bi, Z. Falls, P. Avery, and E. Zurek, J. Am. Chem. Soc. **138**, 1884 (2015).

[41] H. Liu, Y. Li, G. Gao, J. S. Tse, and I. I. Naumov, J. Phys. Chem. C **120**, 3458 (2016).

[42] H. Liu, I. I. Naumov, Z. M. Geballe, M. Somayazulu, J. S. Tse, and R. J. Hemley, Phys. Rev. B **98**, 100102(R) (2018).

[43] G. Gao, A. R. Oganov, Y. Ma, H. Wang, P. Li, Y. Li, T. Iitaka, and G. Zou, J. Chem. Phys. **133**, 144508 (2010).

[44] P. Loubeyre, R. LeToullec, D. Hausermann, M. Hanfland, R. Hemley, H. Mao, and L. Finger, Nature (London) **383**, 702 (1996).

[45] A. Dewaele, F. Datchi, P. Loubeyre, and M. Mezouar, Phys. Rev. B **77**, 094106 (2008).

[46] O. Degtyareva, E. Gregoryanz, M. Somayazulu, H.-k. Mao, and R. J. Hemley, Phys. Rev. B **71**, 214104 (2005).

[47] L. Sun, W. Yi, L. Wang, J. Shu, S. Sinogeikin, Y. Meng, G. Shen, L. Bai, Y. Li, J. Liu *et al.*, Chem. Phys. Lett. **473**, 72 (2009).

[48] M. Einaga, M. Sakata, T. Ishikawa, K. Shimizu, M. I. Eremets, A. P. Drozdov, I. A. Troyan, N. Hirao, and Y. Ohishi, Nat. Phys. **12**, 835 (2016).

[49] P. B. Allen and R. Dynes, Phys. Rev. B **12**, 905 (1975).

[50] G. Eliashberg, Sov. Phys. J. Exp. Theor. Phys. **11**, 696 (1960).

[51] http://hdl.handle.net/10477/79221.

[52] G. Henkelman, B. P. Uberuaga, and H. Jónsson, J. Chem. Phys. **113**, 9901 (2000).

[53] D. Sheppard, P. Xiao, W. Chemelewski, D. D. Johnson, and G. Henkelman, J. Chem. Phys. **136**, 074103 (2012).

[54] P. Giannozzi, J. Phys.: Condens. Matter **21**, 395502 (2009).

[55] L. Zhu, H. Liu, C. J. Pickard, G. Zou, and Y. Ma, Nat. Chem. **6**, 644 (2014).

[56] Y. Li, X. Feng, H. Liu, J. Hao, S. A. Redfern, W. Lei, D. Liu, and Y. Ma, Nat. Commun. **9**, 722 (2018).

[57] H. J. Monkhorst and J. D. Pack, Phys. Rev. B **13**, 5188 (1976).

[58] G. Kresse and J. Furthmüller, Phys. Rev. B **54**, 11169 (1996).

[59] G. Kresse and D. Joubert, Phys. Rev. B **59**, 1758 (1999).

[60] J. P. Perdew, K. Burke, and M. Ernzerhof, Phys. Rev. Lett. **77**, 3865 (1996).

[61] J. Shi, W. Cui, S. Botti, and M. A. L. Marques, Phys. Rev. Mater. **2**, 023604 (2018).

[62] Y. Li, J. Hao, H. Liu, S. T. John, Y. Wang, and Y. Ma, Sci. Rep. **5**, 9948 (2015).